ELSEVIER

Journal of Power Sources 66 (1997) 121–127

JOURNAL OF POWER SOURCES

Electrochemical and thermodynamic studies of nickel electrodes in alkaline electrolytes

Ken-ichi Watanabe [a], Naoaki Kumagai [b]

[a] *Saitama Research Laboratory, Shin-Kobe Electric Machinery Co., Ltd., Okabe-Machi Osato-Gun, Saitama-Ken 369 02, Japan*

[b] *Department of Applied Chemistry and Molecular Science, Faculty of Engineering, Iwate University, Morioka 020, Japan*

Received 1 September 1996; accepted 20 October 1996

Abstract

The nickel electrode is widely used as a positive electrode in rechargeable alkaline batteries. The electrochemical behaviour of nickel hydroxide powders in several kinds of electrolyte is investigated. The open-circuit voltage (OCV) of the nickel oxide electrode in 3 M KOH displays an S-shaped curve in the reduction process. On the other hand, the nickel oxide electrode in 3 M NaOH and 3 M LiOH shows two-step reduction OCV curves. In the first stage, the OCV curves are S-shaped, while in the second stage, the OCV curves are L-shaped. The S-shaped stage of the OCV curve is examined by using thermodynamic considerations. The thermodynamic simulation and experimental results are in fairly good agreement with one fitting parameter ϕ/RT; ϕ is an interaction energy parameter (J mol^{-1}) and RT has the usual significance. The interaction energy parameter (ϕ) is found to increase in the order 3 M LiOH < 3 M NaOH < 3 M KOH. This concluded that the alkaline cation intercalated into the nickel oxide lattice decreases the interaction energy parameter (ϕ).

Keywords: Thermodynamic study; Nickel electrodes; Electrolytes

1. Introduction

A number of topics relating to the nickel electrode in rechargeable alkaline batteries have been extensively studied [1–17]. Although the structure of nickel hydroxide is now well understood [1,2], the electrochemical mechanism of this electrode is still not clear. It seems that five reasons contribute to this situation. They are probably due to the strong dependence of the nickel electrode characteristics on:

1. the electrode types (such as the impregnation type [1,3–13] and pasted type [14–17]);
2. the crystal structure of nickel hydroxide (such as α-$Ni(OH)_2$ [1,2], turbostatic-$Ni(OH)_2$ [2] and β-$Ni(OH)_2$ [1,2,16,17]);
3. the crystallite size of nickel hydroxide [16];
4. the type of additive (such as cobalt, cadmium and zinc [1,2,4–7,15–17]), and
5. the type of electrolyte used in the experiments (such as KOH, NaOH, and LiOH [1,2,4,9–13]).

Carefully controlled experiments are required to clarify the behaviour of these individual components.

In the present study, two forms of nickel hydroxide powder samples with different crystalline sizes and three types of electrolyte (3 M KOH, 3 M NaOH, and 3 M LiOH) are used. The intermittent discharge characteristics of the open-circuit voltage (OCV) are measured. The OCV curves in the reduction process depend on the electrolyte used and the crystalline size of the nickel hydroxide. The OCV curves as a function of the reduction process are compared with the thermodynamic considerations reviewed by Crandall et al. [18] and Barnard et al. [19,20]. The measurement and interpretation of the OCV curves is the subject of this investigation.

2. Experimental

2.1. Preparation of electrode materials and nickel electrode

Nickel foam (2 cm × 2 cm, Sumitomo Electric Industries) was used as the nickel electrode substrate. The following two kinds of β-type nickel hydroxide (β-$Ni(OH)_2$), powders A and B, were used as the positive electrode materials. These samples were obtained from Nihon Kagaku Sangyo Company. Cobalt metal powder (N.V. Union Minière S.A.) was added at 5 wt.% to the hydroxide powders to increase and stabilize the utilization of the active materials [14, 15]. Hydroxypropylmethylcellulose (HPMC) (Shin-Etsu Chemical) and polytetrafluoroethylene (PTFE) dispersion (Daikin Industries) were used as binders.

PII S0378-7753(96)02537-2

The preparation of the nickel electrode has been described in Ref. [16]. The geometrical surface area of the nickel electrode was 4 cm^2 and the weight of nickel hydroxide in powders A and B was about 0.14 g cm^2. These nickel electrodes were spot-welded to a 6 mm nickel ribbon as a current-collector.

2.2. *Analysis of nickel hydroxide powder and electrochemical measurement of nickel electrode*

The apparatus for analysis of the physical properties of nickel hydroxide powder was the same as that used previously [17].

Charge/discharge curves were obtained with a glass beaker cell. Nickel mesh was used as the counter electrode, and three kinds of electrolyte 3 mol l^{-1} KOH (3 M KOH), 3 mol l^{-1} NaOH (3 M NaOH) and 3 mol l^{-1} LiOH (3 M LiOH) were used. The 3 M KOH, 3 M NaOH and 3 M LiOH solutions were prepared using reagent grade chemicals and distilled water. The potential was measured against a Hg/HgO (3 M KOH, 3 M NaOH or 3 M LiOH) reference electrode in the same solution. The electrolysis cell was placed in an incubator held at 20 ± 1 °C. Charging was performed initially at a rate of 7.0 mA cm^{-2} for 6 h. The charging capacity was about 120% of the theoretical capacity of the nickel hydroxide positive electrode. Discharging was then carried out at a rate of 7.0 mA cm^{-2} down to 0.1 V versus Hg/HgO, followed by a recharge at a rate of 7.0 mA cm^{-2} for 6 h. The theoretical capacity of nickel hydroxide is 289 mAh per g of active material by assuming the electrode reaction to be

$$Ni(OH)_2 + OH^- \rightleftharpoons NiOOH + H_2O + e^- \quad (1)$$

Intermittent discharges were then carried out at a rate of 7.0 mA cm^{-2} down to 0.1 V versus Hg/HgO. To reach equilibrium after intermittent discharge, a period of 20 to 60 h at a constant temperature was required in order to obtain a uniform distribution of H^+ ions throughout the working electrode. Equilibrium was considered to have been reached when the OCV was stabilized to less than 0.2 mV h^{-1} at a constant temperature.

3. Thermodynamic theory

In order to describe the OCV curve of the nickel oxide electrode as a function of the reduction process, a thermodynamic theory is used. In Eq. (3), $0<x<1$ is used by assuming the following electrode reactions:

$$Ni(OH)_2 + OH^- \rightleftharpoons NiOOH + H_2O + e^- \quad (2)$$

as

$$H_xNiOOH \rightleftharpoons NiOOH + xH^+ + xe^- \quad (0<x<1) \quad (3)$$

or

$$(Ni(OH)_2)_x(NiOOH)_{1-x} \rightleftharpoons NiOOH + xH^+ + xe^- \quad (4)$$
$$(0<x<1)$$

The x value shows the mole fraction of $Ni(OH)_2$ in the nickel oxide electrode (Eq. (4)).

A thermodynamic theory of metal oxide electrodes has been established by Crandall et al. [18] and Barnard et al. [19,20]. In this work, the equation proposed by Barnard et al. [19,20] is used. The equation was slightly modified in symbols

$$E = E^0 + (RT/F)(\phi/RT)(2x-1) + \varphi(RT/F) \times \ln((1-x)/x) \quad (5)$$

where E is the electrode potential at constant pH(V); E^0 is the standard electrode potential (V); R is the gas constant (J K^{-1} mol^{-1}); T is the absolute temperature (K); F is the Faraday constant (C); x is the mole fraction of $Ni(OH)_2$ in nickel oxide; ϕ is the interaction energy parameter (J mol^{-1}). According to Crandall et al. [18], φ is the proton-electron spatial correlation coefficient and takes a value of 2 if the electron and proton are not closely correlated, and a value of 1 if they are spatially correlated. In Eq. (5), all higher-order terms in x may be neglected [18]. Eq. (5) shows that $E = E^0$ at $x = 0.5$ (145.5 mAh per g of active material discharge in Eq. (1)). Eq. (5) can be transformed into Eq. (6), as follows

$$E - E^0 = (RT/F)(\phi/RT)(2x-1) + \varphi(RT/F) \times \ln((1-x)/x) \quad (6)$$

The values of E–E^0 versus typical values of ϕ/RT are calculated and shown in Figs. 1 and 2. Clearly, the data display S-shaped curves. In particular, when x tends towards 0 or 1, E–E^0 tends towards infinity. The curve for $\phi/RT = 0$ corresponds to the simplified Nernst equation, where mole fractions are used to replace the activity term. On the other hand, the ϕ/RT value of 1, 2 and 4 displays positive deviations from ideality.

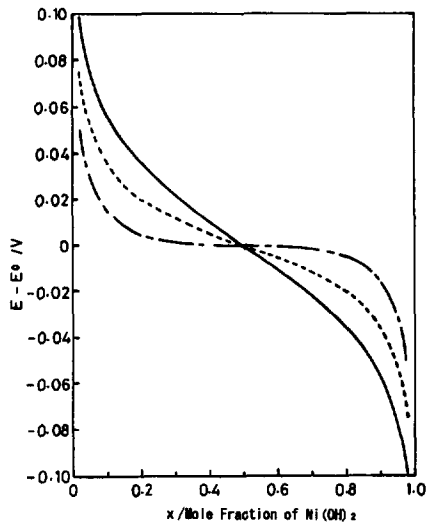

Fig. 1. Plots of $E - E^0$ vs. x in $\varphi = 1$: (———) $\phi/RT = 0$; (- - -) $\phi/RT = 1$, and (– · –) $\phi/RT = 2$.

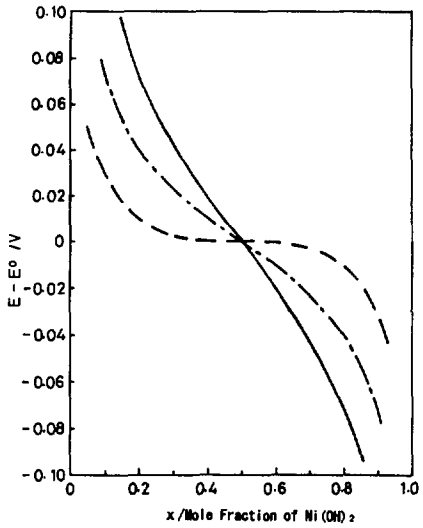

Fig. 2. Plots of $E-E^0$ vs. x in $\varphi=2$: (———) $\phi/RT=0$; (– · –) $\phi/RT=2$, and (— — —) $\phi/RT=4$.

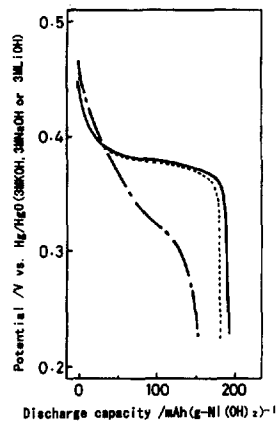

Fig. 3. Discharge curves of sample A at a discharge rate of 7.0 mA cm^{-2}: (———) 3 M KOH; (· · ·) 3 M NaOH, and (– · –) 3 M LiOH.

4. Results

4.1. Physical properties of nickel hydroxide samples

The chemical composition and physical properties of the nickel hydroxide samples are presented in Table 1. The cadmium contents are nearly zero and the cobalt content in sample B is slightly less than that in sample A. The cobalt content in each sample appears to have little effect on the electrochemical characteristics, as shown in Ref. [17]. The mean diameter of these samples is in the range of 14 to 15 μm, and the BET surface areas are between 19 and 38 $m^2\ g^{-1}$.

The structure of the nickel hydroxide powder has already been determined by the X-ray diffraction (XRD) method [16] and is found to be β-type nickel hydroxide (β-$Ni(OH)_2$) of a brucite-type structure with a hexagonal unit cell. The full width of the half-maximum intensity (FWHM) and the d values of the respective samples in the (001), (100) and (101) reflections are listed in Table 2. The FWHM values for sample B are smaller than those of sample A. This suggests that the crystalline size of the nickel hydroxide powder in sample B is larger than that in sample A [21]. Samples A and B exhibit almost the same d_{100} and d_{101} values. On the other hand, the d_{001} values (which indicate the interlayer distance of a brucite-type structure with a hexagonal unit cell) of sample A is slightly larger than that of sample B.

4.2. Electrochemical characteristics of nickel hydroxide electrodes

4.2.1. Constant current charge/discharge curves

Typical discharge and charge curves for sample A in different types of electrolyte (3 M KOH, 3 M NaOH and 3 M LiOH) are given in Figs. 3 and 4. In these experiments, the potential was measured against Hg/HgO electrodes in 3 M

Table 1
Physical properties of nickel hydroxide samples

Sample	Chemical composition			Mean diameter (μm)	BET surface area ($m^2\ g^{-1}$)
	Ni (wt.%)	Co (wt.%)	Cd (wt.%)		
A	61.9	0.19	<0.01	14	38
B	61.7	0.16	<0.01	15	19

Table 2
FWHM and d values in (001), (100) and (101) diffraction lines of nickel hydroxide samples

Sample	(001)		(100)		(101)	
	$FWHM_{001}$ (°)	d_{001} (nm)	$FWHM_{100}$ (°)	d_{100} (nm)	$FWHM_{101}$ (°)	d_{101} (nm)
A	1.095	0.4682	0.450	0.2709	1.153	0.2342
B	0.529	0.4619	0.360	0.2709	0.432	0.2336

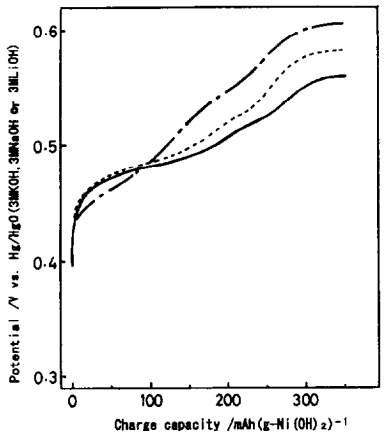

Fig. 4. Charge curves of sample A at a charge rate of 7.0 mA cm^{-2}: (———) 3 M KOH; (· · ·) 3 M NaOH, and (– · –) 3 M LiOH.

KOH, 3 M NaOH or 3 M LiOH in order to eliminate the contamination of each of the electrolytes.

For the initial discharge curves (Fig. 3), it is found that the 3 M LiOH curve is quite different from those of 3 M KOH and 3 M NaOH. The potential in 3 M LiOH is higher than those in 3 M KOH and 3 M NaOH in the discharge capacity range of 0 to about 30 mAh per g of $Ni(OH)_2$. On the other hand, in the discharge capacity region above about 30 mAh per g of $Ni(OH)_2$, the potential in 3 M LiOH is lower than that in either 3 M KOH or 3 M NaOH. The coulombic efficiency in 3 M LiOH is clearly less than that in either 3 M KOH or 3 M NaOH.

For the charge curves (Fig. 4), the potential in 3 M LiOH is lower than that in 3 M KOH and 3 M NaOH in the charge capacity range 0 to about 100 mAh per g of $Ni(OH)_2$. On the other hand, in the charge capacity region above about 100 mAh per g of $Ni(OH)_2$, the potential in 3 M LiOH is higher than that in 3 M NaOH, while that in 3 M KOH is lower than that in 3 M NaOH. In the charge capacity region above about 290 mAh per g of $Ni(OH)_2$, an obvious charge plateau appears. The latter region is caused by the oxygen-evolution reaction [1]

$$2OH^- \rightarrow (1/2)O_2 + H_2O + 2e^- \quad (7)$$

4.2.2. *Intermittent current discharge curves*

Variations in the closed-circuit voltage and quasi-equilibrium OCV of samples A and B are presented in Fig. 5 (3 M KOH), Fig. 6 (3 M NaOH) and Fig. 7 (3 M LiOH) as a function of discharge capacity. In these curves, the coulombic efficiency of sample A is higher than that of sample B. Moreover, the polarization for sample A is lower than that for sample B. These effects would cause the relation between the crystalline size of nickel hydroxide and the proton diffusion in the solid as discussed in Ref. [16].

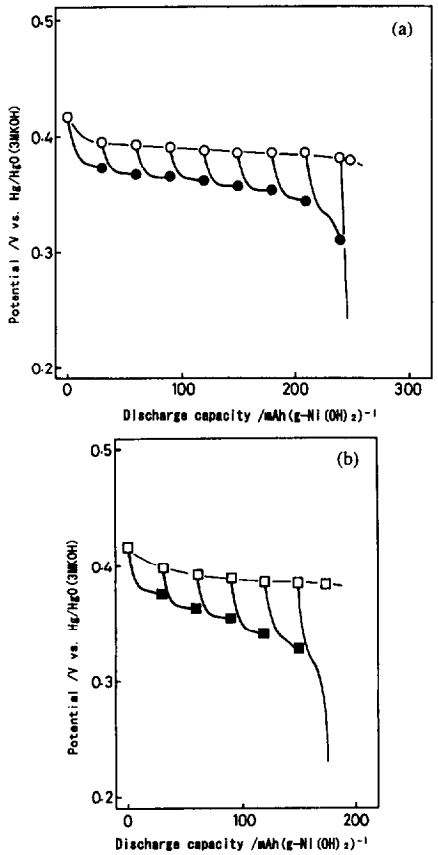

Fig. 5. Intermittent discharge curves of samples A and B. (a) (○) Open-circuit potential and (●) closed-circuit potential for sample A; (b) (□) open-circuit potential and (■) closed-circuit potential for sample B.

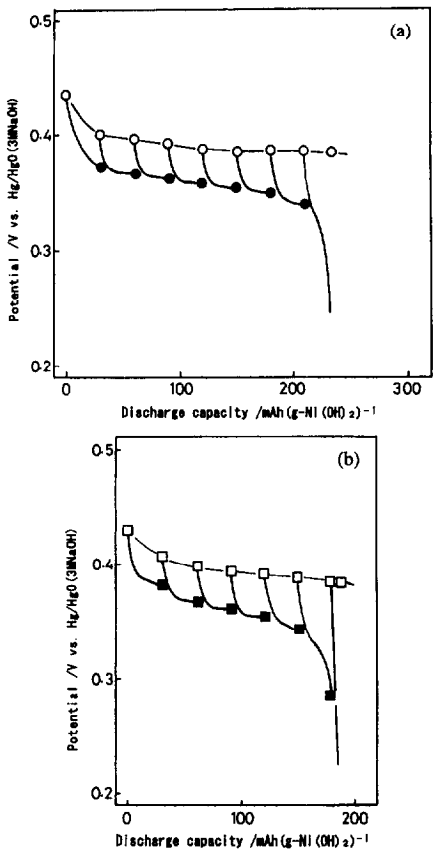

Fig. 6. Intermittent discharge curves of samples A and B in 3 M NaOH. (a) (○) Open-circuit potential and (●) closed-circuit potential for sample A; (b) (□) open-circuit potential and (■) closed-circuit potential for sample B.

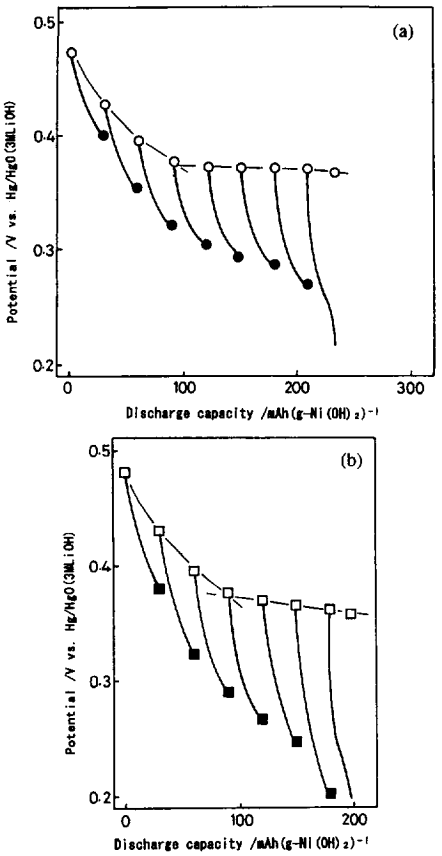

Fig. 7. Intermittent discharge curves of samples A and B in 3 M LiOH. (a) (○) Open-circuit potential and (●) closed-circuit potential for sample A; (b) (□) open-circuit potential and (■) closed-circuit potential for sample B.

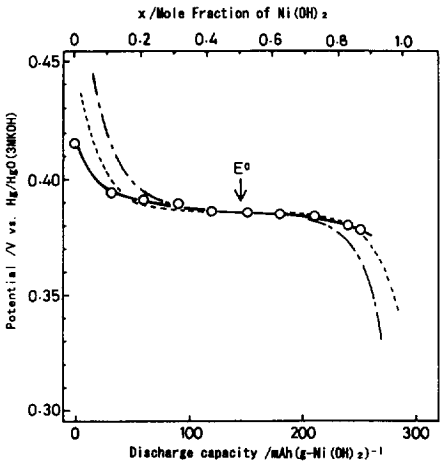

Fig. 8. Comparison of potential vs. discharge state in 3 M KOH (sample A): (○) experimental open-circuit potential; (– – –) calculated ($\varphi=1$, $\phi/RT=2.00$), and (– · –) calculated ($\varphi=2$, $\phi/RT=4.05$).

The OCV potentials in Fig. 5 (3 M KOH) and Fig. 6 (3 M NaOH) decrease with discharge. On the other hand, two-step OCV curves are clearly observed in Fig. 7 (3 M LiOH). In Fig. 7, there is a sharp bend in the OCV curves at 90–100 mAh per g of $Ni(OH)_2$ discharge. In the first stage, the OCV curves decrease with discharge, while in the second stage, the OCV curves remain nearly constant.

5. Discussion

A least-square error fit of Eq. (5) was made with just one fitting parameter ϕ/RT to the experimental OCV data (Figs. 5–7). The typical OCV curves for sample A and the fitted curves are shown in Figs. 8–10 ($\varphi=1$ (broken line), $\varphi=2$ (dashed-and-dotted line)). Note that, the potential ranges in Figs. 5–7 and Figs. 8–10 differ.

In Figs. 8–10, the charged state of the nickel oxide is assumed to be $x=0$. The value of x in the discharge process is calculated from the mass of the nickel hydroxide, the value of the current and the discharge time. The E^0 values in Eq. (5) were obtained experimentally, assuming that the E^0 values were the OCV in $x=0.5$ (145.5 mAh per g of active material discharged in Figs. 8–10). The resulting E^0 values for sample A were 0.386, 0.386 and 0.370 V in 3 M KOH, 3 M NaOH and 3 M LiOH, respectively.

Plots of the experimental OCV curve and the calculated curve in 3 M KOH (broken line, $\varphi=1$, $\phi/RT=2.00$); (dashed-and-dotted line, $\varphi=2$, $\phi/RT=4.05$) are displayed,

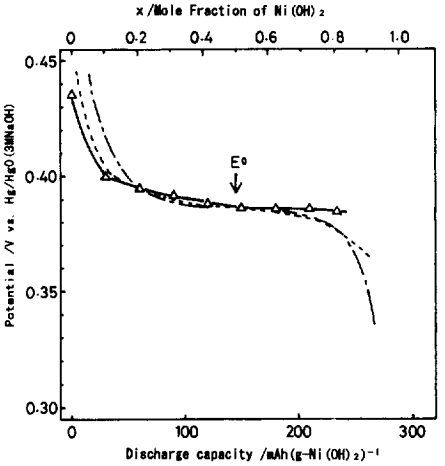

Fig. 9. Comparison of potential vs. discharge state in 3 M NaOH (sample A): (△) experimental open-circuit potential; (– – –) calculated ($\varphi=1$, $\phi/RT=1.80$), and (– · –) calculated ($\varphi=2$, $\phi/RT=4.00$).

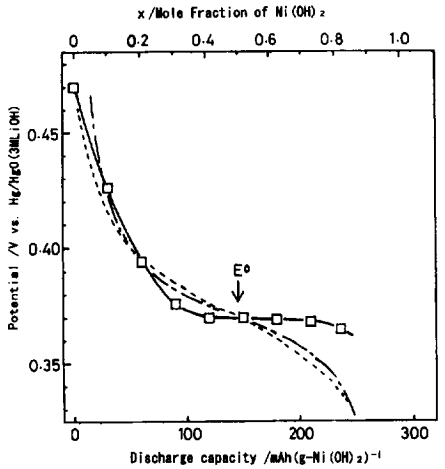

Fig. 10. Comparitson of potential vs. discharge state in 3 M LiOH (sample A): (□) experimental open-circuit potential; (– – –) calculated ($\varphi=1$, $\phi/RT=0.55$), and (– · –) calculated ($\varphi=2$, $\phi/RT=2.95$).

Table 3
ϕ/RT values with $\varphi = 1$ or 2 for nickel hydroxide samples

		ϕ/RT	
		$\varphi = 1$	$\varphi = 2$
Sample A	3 M KOH	2.05	4.05
	3 M NaOH	1.80	4.00
	3 M LiOH	0.55	2.95
Sample B	3 M KOH	1.95	4.00
	3 M NaOH	1.75	3.90
	3 M LiOH	0.30	2.45

in Fig. 8. The fit of the experimental data to the calculated broken line ($\varphi = 1$) is very good. Both the experimental OCV data and the calculated line have an S-shaped curve. Therefore, the discharge reaction of the nickel oxide electrode in 3 M KOH is must likely caused by a one-phase system.

Plots of the experimental OCV curve and the calculated curve in 3 M NaOH (broken line, $\varphi = 1$, $\phi/RT = 1.80$); (dashed-and-dotted line, $\varphi = 2$, $\phi/RT = 4.00$) are displayed in Fig. 9. The fit of the experimental data to the calculated broken-line ($\varphi = 1$) in $0 < x < 0.7$ is fairly good. In particular, the OCV curve has an S-shape in this region. For an x value in excess of 0.7, however, the experimental data have an L-shaped curve; thus, the discharge reaction is possibly a two-phase system.

Plots of the experimental OCV curve and the calculated curve in 3 M LiOH (broken line, $\varphi = 1$, $\phi/RT = 0.55$); (dashed-and-dotted line, $\varphi = 2$, $\phi/RT = 2.95$) are presented in Fig. 10. The fit of the experimental data to the calculated line (the broken line and the dashed-and-dotted line) in $0 < x < 0.5$ is rather good. In particular, the OCV curve is S-shaped in this region. On the other hand, for an x value in excess of 0.5, the experimental data display an L-shaped curve; thus, the discharge reaction is most likely caused by a two-phase system.

The same considerations also apply to sample B. The ϕ/RT values with $\varphi = 1$ or 2 for samples A and B are presented in Table 3. The ϕ/RT value in 3 M KOH is larger than that in 3 M NaOH, while the value in 3 M LiOH is smaller than that in 3 M NaOH. According to Crandall et al. [18], ϕ is the interaction energy parameter. These data show that the interaction energy parameter increase in the order: 3 M LiOH < 3 M NaOH < 3 M KOH.

A comparison of the crystal radius and the hydrated radius of alkaline metals (Li^+, Na^+, K^+) is presented in Table 4 [22]. The crystal radius of Li^+ is the smallest, while that of K^+ is the largest. On the other hand, the hydrated radius of Li^+ is the largest, while that of K^+ is the smallest. Several authors have suggested [1,2,4,13] that the alkaline metal ions (Li^+, Na^+ and K^+) intercalate and de-intercalate in the intersheet region of the layered material of the nickel oxide crystal. The Li^+ ion, which has the smallest crystal radius, should intercalate easily into the nickel oxide crystal; therefore, the intercalated Li^+ ion makes the interaction energy parameter (ϕ) lower. It is more difficult, however, for the K^+ ion (which has the largest crystal radius) to intercalate into the nickel oxide crystal than for the Li^+ ion; thus, the K^+ ion has little effect on the interaction energy parameter (ϕ). It appears that the intercalated alkaline metal ions also affect the continuous charge/discharge curves, as shown in Figs. 3 and 4.

Table 4
Comparison of crystal and hydrated radii of alkali metals [22]

Ion	Crystal radius (nm)	Hydrated radius (nm)
Li^+	0.060	0.382
Na^+	0.095	0.358
K^+	0.133	0.331

The data in Table 3, also show that the ϕ/RT value of sample A is slightly larger than that of sample B when the same electrolyte is used. The crystalline size of the nickel hydroxide powder seems to affect the intercalation of the alkaline ion. The nickel hydroxide with a smaller crystalline size in sample A than that in sample B (Table 2) displays a higher coulombic efficiency and lower polarization in the discharge process (Figs. 5–7). Nickel hydroxide powder with a smaller crystalline size has been reported [16] to give a higher proton diffusion coefficient. In sample A, in which the proton easily intercalates and de-intercalates, the intercalation of the alkaline ion appears to be restricted. The amount of intercalated alkaline ion in sample A is smaller than that in sample B and, accordingly, has little effect on the interaction energy parameter (ϕ).

The reason why the intercalated alkaline ion affects the interaction energy parameter (ϕ) is not yet clear. Since these effects are important for the performance of the nickel oxide electrode, more study of the mechanism is necessary.

References

[1] S.U. Falk and A.J. Salkind, *Alkaline Storage Batteries*, Wiley, New York, 1969.
[2] P. Oliva, J. Leonardi, J.F. Laurent, C. Delmas, J.J. Braconnier, M. Figlarz, F. Fievet and A. Guibert, *J. Power Sources, 8* (1982) 229.
[3] D.M. MacArthur, *J. Electrochem. Soc., 117* (1970) 729.
[4] D.A. Corrigan and S.L. Knight, *J. Electrochem. Soc., 136* (1989) 613.
[5] D.F. Pickett and J.T. Maloy, *J. Electrochem. Soc., 125* (1978) 1027.
[6] D.H. Fritts, *J. Electrochem. Soc., 129* (1982) 118.
[7] M. Oshitani, T. Takayama, K. Takashima and S. Tsuji, *J. Appl. Electrochem., 16* (1986) 403.
[8] R.D. Armstrong, G.W.D. Briggs and E.A. Charles, *J. Appl. Electrochem., 18* (1988) 215.
[9] E.J. Rubin and R. Baboian, *J. Electrochem. Soc., 118* (1971) 428.
[10] Z. Takehara, M. Kato and S. Yoshizawa, *Electrochim. Acta, 16* (1971) 833.
[11] G. Halpert and L. May, *J. Electrochem. Soc., 124* (1977) 1482.
[12] R.D. Armstrong, A.K. Sood and M. More, *J. Appl. Electrochem., 15* (1985) 603.

[13] P.V. Kamath and M.F. Ahmed, *J. Appl. Electrochem., 23* (1993) 225.
[14] I. Matsumoto, M. Ikeyama, T. Iwaki and H. Ogawa, *Denki Kagaku, 54* (1986) 159.
[15] I. Matsumoto, M. Ikeyama, T. Iwaki, Y. Umeo and H. Ogawa, *Denki Kagaku, 54* (1986) 164.
[16] K. Watanabe, T. Kikuoka and N. Kumagai, *J. Appl. Electrochem., 25* (1995) 219.
[17] K. Watanabe, M. Koseki and N. Kumagai, *J. Power Sources, 58* (1996) 23.
[18] R.S. Crandall, P.J. Wojtowicz and B.W. Faughnan, *Solid State Commun., 18* (1976) 1409.
[19] R. Barnard, C.F. Randell and F.L. Tye, *J. Appl. Electrochem., 10* (1980) 127.
[20] R. Barnard, C.F. Randell and F.L. Tye, *J. Electroanal. Chem., 119* (1981) 17.
[21] B.D. Cullity, *Elements of X-ray Diffraction*, Addison–Wesley, Reading, MA, 1956.
[22] E.R. Nightingale, Jr., *J. Phys. Chem., 63* (1959) 1381.